Contract No.:

This manuscript has been authored by Battelle Savannah River Alliance (BSRA), LLC under Contract No. 89303321CEM000080 with the U.S. Department of Energy (DOE) Office of Environmental Management (EM).

Alloying of U-Al-SS as a Simulant for Pu-Al-SS Alloying

L. C. Olson, Westinghouse Electric Co., Hopkins, South Carolina
R. A. Pierce and H. M Ajo, Savannah River National Laboratory, Aiken, South Carolina

Abstract

The Savannah River National Laboratory (SRNL) evaluated several options for disposition of stainless-steel clad plutonium metal, particularly Pu-10.6 atomic % Al (Pu- 1.3 wt % Al) alloy fuel. One technology considered was alloying fuel with stainless steel (SS). The goal of the alloying would be to make a SS-Pu alloy that was a non-proliferable waste form with secondary Pu rich microencapsulated regions distributed throughout the refractory stainless steel. The microencapsulation of the Pu regions should therefore allow the waste form to meet the requirements for a low attractiveness waste as defined by the United States Department of Energy (DOE). Pu bearing alloys at these levels could potentially be suitable for disposal at WIPP. Four metal ingots were successfully fabricated using U and Al as a surrogate for Pu-Al. The U was distributed and microencapsulated by the alloy matrix, thereby setting the stage for subsequent tests using SS-clad fuel elements containing Pu-10.6Al.

Keywords

alloy waste form, metal waste form, microencapsulant, microstructure

I. Background

The Savannah River National Laboratory (SRNL) demonstrated an actinide alloying process to produce Pu waste forms. The baseline process would generate SS-Pu ingots of about 8-kg with a Pu loading of <5 wt %, which was determined to be the mass for an alloy ingot at the maximum target Pu loading of 350-g. Laboratory-scale tests were conducted to verify expectations about alloying actinides with only 304SS because previous research targeted more complex alloys. U was used as a surrogate for Pu in early work. Test results for full-scale Pu-bearing ingots will be reported in a subsequent paper. The goal of the alloying would be to make a SS-Pu alloy that was a non-proliferable waste form with secondary Pu rich microencapsulated regions distributed throughout the refractory stainless steel. The microencapsulation of the Pu regions should therefore allow the waste form to meet the requirements for a low attractiveness waste as defined by the United States Department of Energy (DOE). The waste-form is envisioned to be viable for both irradiated or unirradiated Pu.

The DOE complex has been researching metal waste forms (MWF) from U based spent fuels for several decades to sequester actinides in Al, steels, and Zr based alloys. These MWFs are primarily SS with up to 20 wt % Zr and U. The INL MWF phases are dictated by the fuel compositions and enrichments used in the Experimental Breeder Reactor Two (EBR-II) fuel being dispositioned. SRNL has conducted extensive research in dilution of fissile materials and production of non-proliferable MWFs since the late 1990s, including evaluating disposition of U-Al spent fuel in Al melts.[1] Fe-based MWFs were investigated to immobilize metallic radioactive species expected from electrometallurgical treatment methods.[2] The goal of this work is to produce a MWF that meets the requirements for a low attractiveness waste, Level D or E, as defined in DOE-STD-1194-2011.

The MWF formulation for the current work has few preconditions because the fuel under consideration has a relatively pure Pu-10.6Al alloy. According to the Fe-Pu phase diagram, Pu should form an intermetallic Fe_2Pu phase in SS with some limited solid solutioning. Previous research has shown that SS-Zr-Pu and SS-Zr-U alloy microstructures look and behave similar with the same apparent phases.[3,4] Furthermore, SS-Zr-Pu and SS-Zr-U alloys were made with Pu and U concentrations up to 10 wt % and 11 wt %, respectively, that maintained expected microstructures.[3]

II. Experimental Procedure

IIA. Materials

Standard 304SS was used for alloying. The composition assumed for calculations was 66.6% Fe, 20.0% Cr, 10.5% Ni, 2.0% Mn, 0.8% Si, and 0.1% C. The Zr rod (99.2% purity metals basis) was obtained through Goodfellow (part #356-468-02) and did not have the Hf component removed (Hf >0.2%). The Al foil was standard commercially available foil.

The U composition used for laboratory-scale melts contained 400 ppm C, 125-225 ppm Fe, 125-225 ppm Si, and 50 ppm N_2.[1] All other impurities were below 20 ppm. The U component for the laboratory-scale alloys required an oxide removal step with acid just prior to alloy fabrication due to the tendency of U to rapidly form a very stable oxide in air at room temperature. The U addition was taken from lathe turnings obtained from a U target originally manufactured to be used in a Pu production reactor, and hence had a well-known pedigree. The turnings were about 5 mm wide, 1 mm thick, and could be 5 cm to >0.5 m long.

The crucibles for the laboratory-scale tests were 26 mm tall, 19 mm in diameter with a volume of 5 mL. They were fabricated from Y_2O_3-stabilized ZrO_2 (YSZ) by McDanel Advanced Ceramic Technologies LLC (Part# ZCN4758).

II.B. Test Matrix

Table I is a list of the weights of components used to make the first laboratory-scale alloys. Test #1 did not provide any data relevant to this paper. The first test alloy composition (#2) in Table I was to determine if Zr was necessary to microencapsulate the actinide, and the second alloy composition (#3) was to ensure the minor Al content from the Pu-Al alloy would not affect the microencapsulation. Alloys #4 and #5 evaluated the need for and effect of Zr concentration on the microencapsulation of actinides.

Table I. Laboratory-scale test matrix

Alloy	304L SS (g)	U* (g)	Al (g)	Zr (g)
#2 SS-1U	20.2554	0.877	-	-
#3 SS-1U-0.1Al	20.8817	0.772	0.0097	-
#4 SS-1U-0.1Al-1Zr	19.4690	0.854	0.0101	0.3343
#5 SS-1U-0.1Al-4Zr	20.3232	0.915	0.0105	1.4087

*A different scale than used for the other components, with a lower precision, was used to weigh the U component in the contaminated area where the work was performed.

The goal of the alloy fabrication and design of the test matrix was to allow for compositional analysis to determine that fuel elements could be alloyed with 304SS exclusively or with SS-Zr, with U used as a surrogate for Pu. Previous research by Keiser had demonstrated that Pu behavior in SS-15 wt % Zr alloys was like that of U, and hence U could be considered a microstructural surrogate for Pu.[3] Alloy #2 examined exclusively 304SS and U to determine if U would form a microencapsulant by itself without the Zr used in previous MWF research. In the previous research on MWFs, actinides were found to collocate with the Zr phase, substituting interstitially at Zr sites of the $ZrFe_2$ intermetallics.[3] Alloy #3 was like alloy #2 but added Al to ensure the minor amount in the fuel meat could be tolerated. To determine if Zr was needed to form a microencapsulant and the effect of the Zr concentration on the areal density of the Zr enriched microencapsulating composition, alloy #4 and alloy #5 added one and four atomic % Zr, respectively, to the composition used in alloy #3. The laboratory-scale alloys were examined for compositional variations following fabrication.

II.C. Laboratory-scale Furnace Configuration

Equipment and fabrication techniques refined in earlier MWF work performed at SRNL were used for this project.[5] The general scheme for the furnace argon gas flow is shown in Figure 1. The day before alloy fabrication, the furnace was calcined under vacuum at 1500 °C for 2 hours to remove moisture from the furnace. After calcining, the furnace was kept under vacuum until loading of the crucibles.

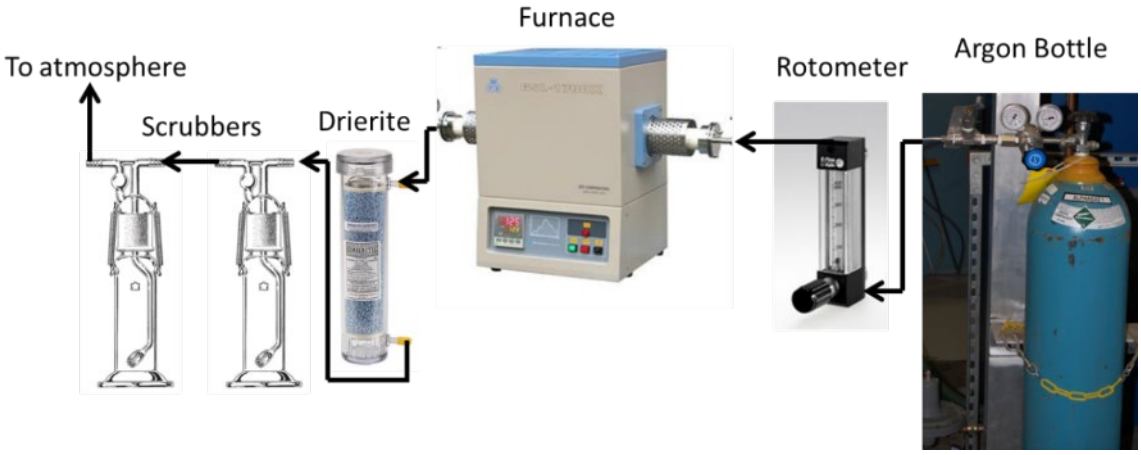

Figure 1. Furnace gas flow set-up

The crucible components (other than the U) were either measured out the day before testing and kept under vacuum, or the day of testing. The U metal pieces were prepared as described previously. The U metal pieces were placed in the bottom of YSZ crucibles, with all other components loaded on top of them. If Al foil was used, that was placed on top of the U pieces, then the 304SS rods were placed in, followed by the Zr. Figure 2 shows the four YSZ crucibles loaded minus the U. A list of the materials loaded into each test alloy is provided in Table I.

Figure 2. Laboratory-scale alloy crucibles before heating

Once the alloy components were introduced into the furnace, the furnace tube was evacuated and flushed with argon, repeating the flush and evacuation procedure three times. The tube was evacuated for heating up to approximately 1500 °C with a constant argon flow of 0.2 scfh (standard cubic feet per hour) to aid in impurity removal. Above approximately 1500 °C, a constant argon gas flow of about 0.2 scfh was introduced through the tube furnace at near atmospheric pressure.

YSZ crucibles were used to hold the alloying components for fabrication. These crucibles could be loaded up to seven at a time into an alumina ashing boat. Ta foil was cut to fit in the boat and lay on top of the crucibles to act as a lid. In practice, the four alloys of the test matrix were loaded in a single test. Additional Ta foil was wrapped around the interior of the alumina ashing boat (around the crucibles), and a second ashing boat was placed on top of the crucibles to act as a cover. The Ta foil wrap/lid act as a scavenger for residual oxygen. The laboratory-scale alloys were approximately 20 g each.

The heating profile for alloy fabrications involved heating the interior of the tube from ambient temperature to 1650 °C at a rate of 5 °C/min, holding at 1650 °C for 1 hour, cooling to 540 °C at a rate of 5 °C/min, and then cooling the furnace at its fastest rate possible. Once cooled, the alloys were removed from the furnace and broken out of the YSZ crucibles, resulting in "button" shaped alloys (Figure 3) about 1.5 cm in diameter and 1.5 cm in height. The alloys were then prepared for analysis using standard metallography techniques described below.

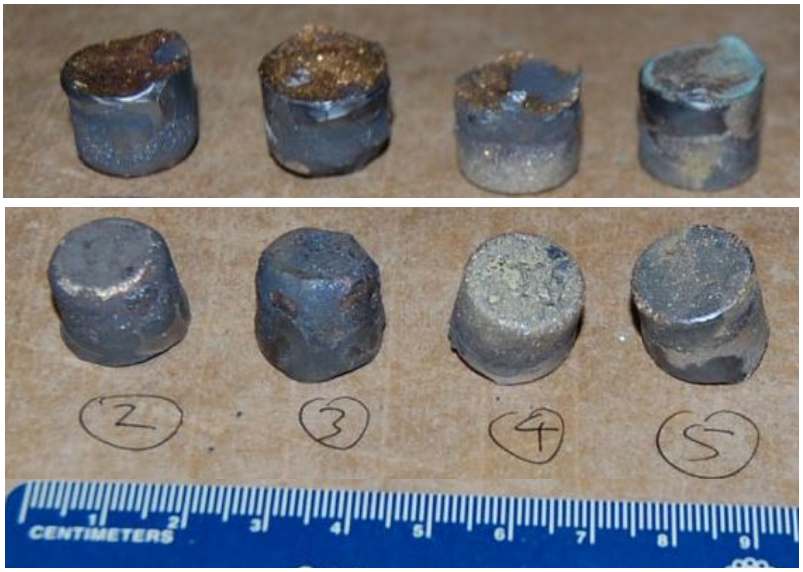

Figure 3. Post fabrication photograph of the test samples

III. Results and Discussion

The laboratory-scale alloys were first examined gravimetrically and visually. Next, they were sectioned at roughly the axial mid-line, mounted, polished, and analyzed by scanning electron microscopy / energy dispersive x-ray spectroscopy (SEM/EDS). The SEM/EDS was to determine general tendencies for segregation of elements towards specific characteristic compositions. It is possible that the four main identified characteristic compositions are a phase or spectrum of phases centered about the main compositions previously identified.[3,4] Further analyses such as XRD, TEM, or EBSD could allow for such a determination. Caution is prudent when looking at EDS data since the region immediately under the surface of the EDS measurement point may have a different composition not observable via backscattered electrons (BSE). Using experimentally calculated diffusion coefficients for Cr, Mn, and Ni, in molten Fe at 1600 °C,[6] and Equation 1 for the effective penetration depth to the right of the Matano plane,[7] the penetration depth for these constituents can be conservatively estimated to range approximately 0.61 cm (Cr) to approximately 0.78 cm (Ni) at 1.5 hours and 1600 °C. The penetration depths of U (and Pu) are expected to be similar in scale to the experimental values. Higher concentrations of U (and Pu) throughout the ingots, than those estimated solely from the liquid diffusion coefficients, could come from the higher hold temperature, time at high temperatures during heating and cooling, mixing caused by convection or entrained gas, and faster diffusion pathways such as at surfaces and grain boundaries. Therefore, good distribution of the U is expected in the smaller ingots.

$$D_{i,R} = \sqrt{2 \cdot \widetilde{D}_{i,R} \cdot t} \qquad \text{Equation 1}$$

Figure 4 identifies the four principal compositions regions (numbered 1-4) found in the alloys that will be discussed. These composition regions tended to partition similar elements.

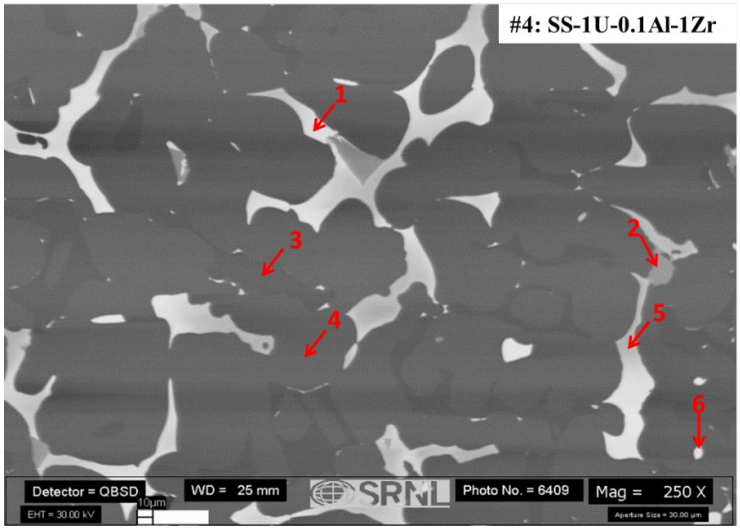

Figure 4. Laboratory-scale alloy showing typical microstructure

Zr, U, and Pu all have similar metallic radii, which are dissimilar to the main 304SS constituents: Fe, Ni and Cr. Therefore, Zr, U, and Pu are likely to be rejected from the steel upon solidification and behave similar in the resulting complex alloy. In Figure 4, the brightest regions like those of Region 1 represent a U-Ni-Fe dominated composition. Region 2 points to the region corresponding to a near Zr-Ni-2Fe composition. Up to three phases with similar compositions have been identified making up the Zr-Fe intermetallics in previous MWF research.[4] It is believed the formation of the $(Zr, U, Pu)_X(Fe, Ni)_Y$ compositions (possibly intermetallics) occurs out of the liquid remaining in the interdendritic regions based on the SEM images. Region 3 is hypothesized to be a ferritic steel with no capacity for U. Based on earlier EBR-II MWF research[8,9,10] δ ferrite can form either from the partial solid-state transformation of dendritic δ ferrite to austenite or during coupled growth with austenite.

The Schaeffler diagram,[11] which is used to predict phase stability in welds in stainless steel, indicates that the 304SS composition is in the 5% ferrite area (approximately 21.2% equivalent Cr, approximately 14.7% equivalent Ni), indicating a microstructure of primary austenite with ferrite dendrites. Zr, U, and Pu could be ferrite stabilizers but are probably too big to fit within the gamma (ferrite) or alpha (austenite) phases. Austenite is a face-centered cubic structure, and other elements tendency to form face-centered cubic could also have an impact on their inclusion into that structure. Pure Zr, below 862 °C has a hexagonal close packed structure, and above a body centered cubic structure. For pure U, an orthorhombic structure is stable up to 668 °C, then tetragonal from 668 °C to 775 °C, and finally body-centered cubic from 775 °C to melting. Pu has six normal allotropes between room temperature and its melting point, starting with a simple monoclinic, then body-centered monoclinic, followed by face-centered orthorhombic, then face-centered cubic, body-centered tetragonal, and finally body-centered cubic. Region 4 is representative of a composition region hypothesized to be an austenitic steel and likewise has no capacity for U (or Zr and Pu). Region 5 represents a section of region 1 that contains less U than regions 1 and 2, and commonly is only present in alloys with high Zr:U ratios. Region 6 is likely an interdendritic region like region 1 or 2 seen from a different orientation.

The U, Pu, and Zr rich regions that can form are not obvious and are dependent on the concentrations of those elements in the interdendritic regions, which are also dependent of cooling rates. Slower cooling allows for more stable phases to form. Faster cooling, such as chill casting, could suppress the formation

of multiple phases. In binary alloys, Pu can form stable $PuNi_2$ and $PuFe_2$ phases that melt at approximately 1210 and 1240 °C, respectively, but also lower melting point eutectics that can melt approximately 413-415 °C.[12] Considering the low levels of actinides being added to the steel, they would be difficult to remove from the surrounding steel without melting it. Based on the SS-U SEM/EDS analysis to date that will be discussed, it does not appear that the low melting point actinide eutectics formed.

III.A. Uniformity

Large area EDS raster analyses were performed at the top, center, and the bottoms of the alloys to determine if the U and other metals were incorporated uniformly into the melt and distributed uniformly throughout the ingots. The theoretical atomic percent of each element as determined by the masses added to the crucibles and using a typical composition for 304SS (66.6% Fe, 20.0% Cr, 10.5% Ni, 2.0% Mn, 0.8% Si, and 0.1% C) are shown in Table II to compare with the large area EDS measurements. Given the semiqualitative nature of the EDS data and limitations on accuracy at low concentrations, the alloying constituents, including the U, appear to have mixed uniformly throughout the small ingots. The most likely explanation for the lower atomic % levels of U in the ingots is first the low accuracy of EDS for determining low levels of elements and U oxidation prior to incorporation into the alloy melt. Uranium oxidation, difficulty wetting the oxidized U surface by the alloy melt, and the small melt size that led to a smaller force pressing down on the oxidized U (and thereby breaking through the oxidized crust on the U), are believed to at least partially explain the difficulty fabricating alloys at the batched U concentrations.

Table II. Alloys #2-#5 calculated and measured compositions

#2 SS-1U						
	Al	**Cr**	**Fe**	**Ni**	**Zr**	**U**
***As-batched Atomic %**	-	20.8	64.5	9.7	-	1.0
Top EDS Atomic %	-	19.3	71.7	8.6	-	0.5
Center EDS Atomic %	-	13.9	74.8	10.8	-	0.4
Bot. EDS Atomic %	-	17.3	72.7	9.3	-	0.7
Average EDS	**-**	**16.8**	**73.1**	**9.6**	**-**	**0.5**
Standard deviation	-	2.7	1.6	1.2	-	0.1
#3 SS-1U-0.1Al						
	Al	Cr	Fe	Ni	Zr	U
***As-batched Atomic %**	0.1	20.8	64.6	9.7	-	0.8
Top EDS Atomic %	0.5	19.6	71.2	8.4	-	0.3
Center EDS Atomic %	0.0	19.6	71.4	8.6	-	0.5
Bot. EDS Atomic %	0.6	19.5	71.1	8.3	-	0.5
Average EDS	**0.4**	**19.5**	**71.3**	**8.4**	**-**	**0.4**
Standard deviation	0.3	0.0	0.1	0.1	-	0.1
#4 SS-1U-0.1Al-1Zr						
	Al	Cr	Fe	Ni	Zr	U
***As-batched Atomic %**	0.1	20.6	63.8	9.6	1.0	1.0
Top EDS Atomic %	-	20.2	70.8	7.8	1.0	0.3
Center EDS Atomic %	-	19.3	70.7	8.3	0.9	0.7
Bot. EDS Atomic %	-	19.1	69.7	8.5	1.7	0.9
Average EDS	**-**	**19.5**	**70.4**	**8.2**	**1.2**	**0.6**
Standard deviation	-	0.6	0.6	0.4	0.5	0.3
#5 SS-1U-0.1Al-4Zr						
	Al	Cr	Fe	Ni	Zr	U
***As-batched Atomic %**	0.1	20	61.9	9.3	3.9	1.0
Top EDS Atomic %	0	18.5	68.5	8.3	3.4	1.2
Center EDS Atomic %	0	18.4	68.6	8.6	3.3	1.2
Bot. EDS Atomic %	0	18.5	68.5	8.3	3.4	1.2
Average EDS	-	18.4	68.6	8.4	3.4	1.2
Standard deviation	-	0.1	0.0	0.2	0.1	0.1

*As-batched compositions were not renormalized to just the 5 or 6 elements normalized for in the EDS results. Renormalization would lead to higher values for the reported elements.

Determining concentrations of elements using large area EDS raster scans, as used in Table II, is best thought of as an engineering approximation. A more accurate method using SEM/EDS would be to determine the U concentration in the individual composition regions, then calculate the weighted average U concentration in the alloy based on the U bearing regions areal density. The apparent spectrum of U-bearing regions or concentration gradients within specific regions made this technique impractical.

The U metal used to make the alloys was cleaned of oxides immediately before fabrication of the alloys. However, it was still observed that the U metal pieces were starting to form an oxide layer during the weighing steps, and more oxidation likely occurred prior to a vacuum being established in the furnace tube and from residual moisture in the tube furnace and tube insulation blocks. These oxide layers could have impacted U incorporation into the alloys.

III.B. Microstructure

SEM/EDS was used to identify distinct composition regions present within the microstructure of the different alloys. There were three distinct composition regions in alloys #2 and #3, and four distinct composition regions when Zr was present in alloys #4 and #5. Figure 5 shows the general morphology visible in the SS-U series scoping alloys at low magnification. Figure 6 presents a higher magnification of the alloys to better exhibit major morphological features.

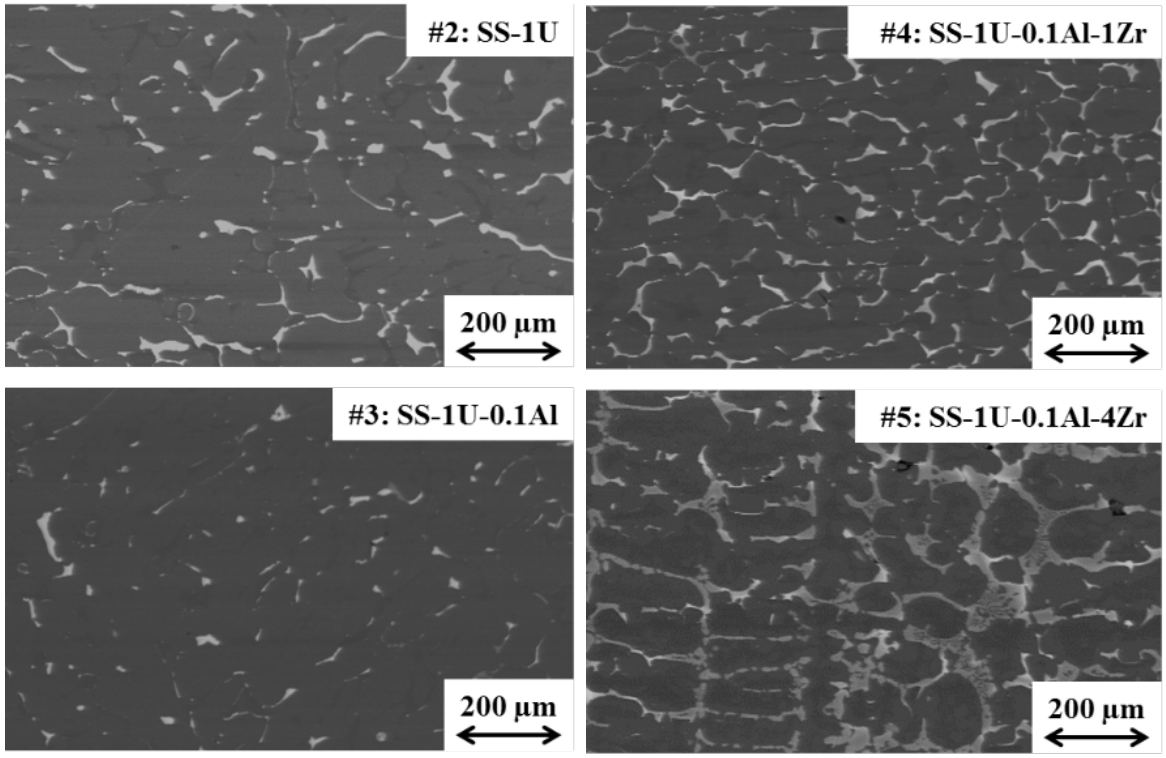

Figure 5. Laboratory-scale low magnification cross-section BSE SEM

U was located primarily in regions with an apparent composition near U-Ni-2Fe. The U-Ni-2Fe composition regions appeared as bright interdendritic regions in BSE SEM and are spread throughout the alloys and encapsulated by the primary steel phase. The U-Ni-2Fe region is identified by Point 1 in Figure 4, and its compositional variance in the alloys tabulated in Table II. When Zr was present, minor amounts of Zr also located to this region.

It has been found previously that when Zr is present, there are at least three phases that can make up a U rich Zr-Fe phase distribution or spectrum.[4] Table IV summarizes a near Zr-Ni-2Fe composition that may encompass the Zr-Fe phase distribution mentioned in prior literature. The Zr-Ni-2Fe like region is Point 2 in Figure 4. This composition appears as grey interdendritic regions when compared to the near U-Ni-2Fe composition in BSE SEM, often is adjacent to it, and is also spread throughout the alloys and encapsulated by the primary steel. The Zr bearing composition in Table IV may partially fit into this category. Furthermore, in some alloys with Zr, the present authors have observed the Zr-Fe compositions can exhibit distinctly different U loadings, and brighter Zr-Fe regions, or Zr-Fe regions with gradients in brightness can appear with the brighter regions signifying a higher U loading.

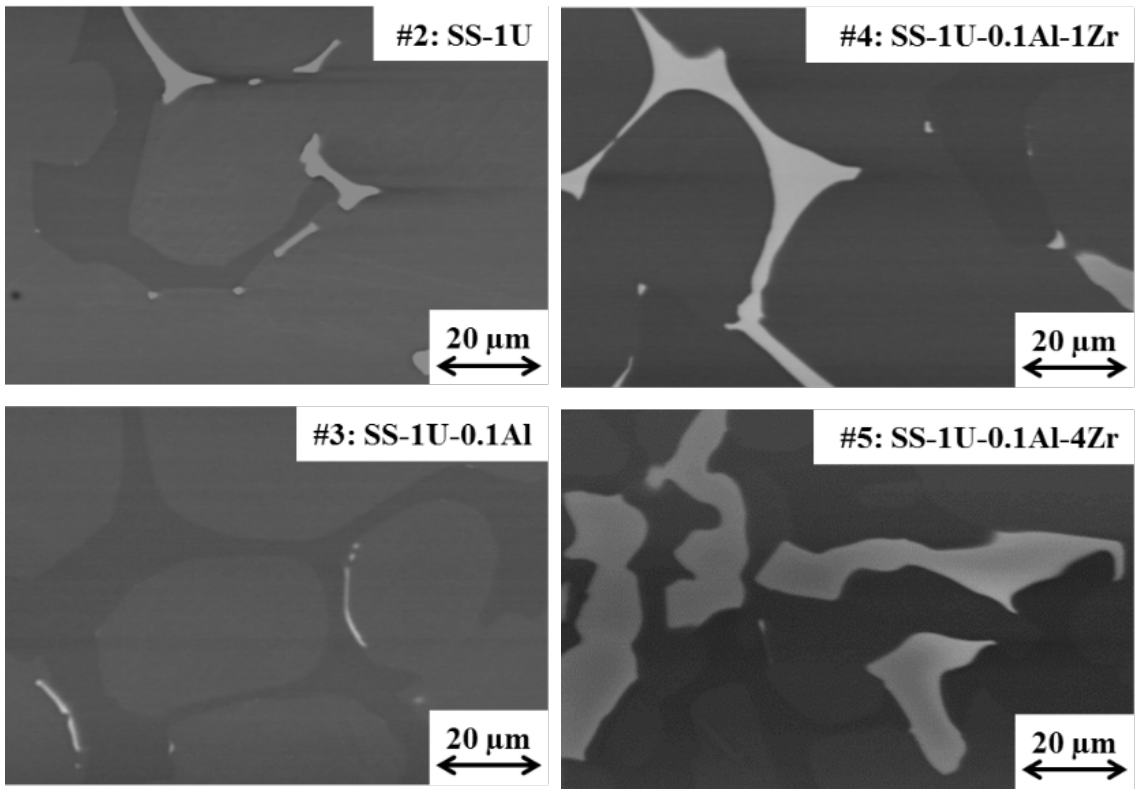

Figure 6. Laboratory-scale higher magnification cross-section BSE SEM

Table III. EDS point scans of U-Ni-2Fe like (U rich) regions

U-Ni-2Fe regions (U Rich) (atomic %)					
Alloy	Cr	Fe	Ni	Zr	U
(#2) SS-1U	2.6	44.6	22.6	-	30.1
[a]Std. Dev. (3)	1.0	2.8	1.6	-	2.2
(#3) SS-1U-0.1Al	2.8	31.2	14.0	-	52.0
[a]Std. Dev. (3)	0.8	23.0	12.2	-	35.9
(#4) SS-1U-0.1Al-1Zr	2.6	42.1	22.4	4.2	28.6
[a]Std. Dev. (3)	0.1	1.7	0.9	1.2	2.1
(#5) SS-1U-0.1Al-4Zr	4.0	47.5	19.0	7.8	21.8
[a]Std. Dev. (3)	0.9	1.0	1.4	4.0	4.0

[a]The number in parenthesis next to the Std. Dev. is the sample size

Table IV. EDS point scans of Zr-Ni-2Fe like (U poor) regions

Zr-Ni-2Fe regions (U Poor) (atomic %)					
Alloy	Cr	Fe	Ni	Zr	U
(#4) SS-1U-0.1Al-1Zr	8.0	57.0	15.7	17.2	2.1
[a]Std. Dev. (3)	0.3	0.8	0.4	0.2	0.4
(#5) SS-1U-0.1Al-4Zr	4.7	53.3	19.3	19.1	3.6
[a]Std. Dev. (3)	0.2	0.6	0.4	1.2	1.2

[a]The number in parenthesis next to the Std. Dev. is the sample size

If the Zr content is high enough (such as in alloy #5), then as the alloy cools, the Zr can concentrate enough in the interdendritic regions to form a eutectic, with a characteristic microstructure. In the binary Zr-Fe phase diagram, the high melting point (1337 °C) eutectic forms at 90.2 atomic % Fe, and a low melting (928 °C) point eutectic forms at approximately 24 atomic % Fe. For the high Zr content alloy #5, a microstructure consistent with eutectic formation was observed and is pointed out in Figure 7. EDS analysis of these near Zr-Ni-2Fe composition regions found that for this alloy (in Table IV), the Fe + Ni content is approximately 73% (hypothesized to perhaps be a corollary to the Fe only content in the Fe-Zr phase diagram).

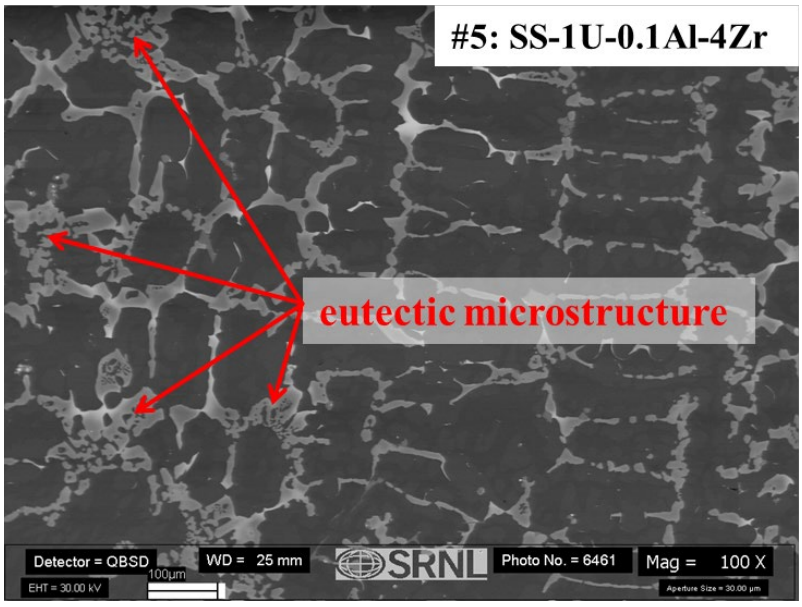

Figure 7. Microstructure in #5 consistent with eutectic formation

Region 3 in Figure 4 may be a ferritic phase, and a similar Fe-rich steel composition was found in all four of the SS-U alloys. There is little elemental variance in this composition region, as evidenced in Table V. This composition region appears often as an interdendritic region adjacent to the near U-Ni-2Fe compositions or the near Zr-Ni-2Fe compositions, and on the edges of the primary matrix steel composition. This region is hypothesized to be ferritic due to its lower Ni content and higher Cr content than the primary steel matrix, which are both features associated with ferrite. There appeared to be more of the potential ferrite in the higher Zr content #5 alloy; Zr is known to be a ferrite stabilizer by forming carbides (or carbonitrides) with carbon, and unbound carbon is an austenite stabilizer.

Table V. EDS point scans of Fe-rich composition

Fe-rich Steel composition (atomic %)					
Alloy	Cr	Fe	Ni	Zr	U
(#2) SS-1U	24.3	70.9	4.8	-	0.0
[a]Std. Dev. (3)	0.2	0.2	0.0	-	0.0
(#3) SS-1U-0.1Al	26.9	69.1	4.0	-	0.0
[a]Std. Dev. (3)	0.3	0.3	0.1	-	0.0
(#4) SS-1U-0.1Al-1Zr	25.1	70.7	4.2	0.0	0.0
[a]Std. Dev. (3)	0.3	0.3	0.2	0.0	0.0
(#5) SS-1U-0.1Al-4Zr	23.5	72.2	4.3	0.0	0.0
[a]Std. Dev. (3)	0.4	0.4	0.1	0.0	0.0

[a]The number in parenthesis next to the Std. Dev. is the sample size

Region 4 in Figure 4 may be an austenitic steel region, and it was found in all four of the SS-U alloys. This was the dominant distinct composition region in all the alloys and encapsulated the other distinct composition regions and notably the U bearing composition regions (with U being a surrogate for Pu). Table VI shows the EDS measurements taken of this distinct steel composition. All the alloys studied had a large Fe component which was primarily where the steel addition segregated. It is hypothesized that this composition may be austenite due to its lower Cr content and higher Ni content, compared to the hypothesized ferrite.

Table VI. EDS point scans of Cr-Ni rich steel

Cr-Ni rich Steel (atomic %)					
Alloy	Cr	Fe	Ni	Zr	U
(#2) SS-1U	16.3	73.5	10.1	-	0.0
[a]Std. Dev. (3)	0.1	0.2	0.1	-	0.1
(#3) SS-1U-0.1Al	17.9	72.6	9.5	-	0.0
[a]Std. Dev. (3)	0.3	0.4	0.3	-	0.0
(#4) SS-1U-0.1Al-1Zr	17.8	73.6	8.7	0.0	0.0
[a]Std. Dev. (3)	0.2	0.4	0.4	0.0	0.0
(#5) SS-1U-0.1Al-4Zr	17.3	74.9	7.8	0.0	0.0
[a]Std. Dev. (3)	0.2	0.2	0.1	0.0	0.0

[a]The number in parenthesis next to the Std. Dev. is the sample size

IV. Conclusions

Research was successfully undertaken to evaluate the separation and microencapsulation of distinct U enriched regions within a steel matrix. Laboratory-scale melts using U were successfully produced with and without Zr metal added. These results indicated that SS-U alloying with microencapsulation and distribution should be possible without Zr. If Zr is used, only 1 at % Zr would be needed to ensure microencapsulation of the U-bearing phase. The alloys have the characteristics of waste forms that are suitable for disposal at WIPP.

V. References

[1] Vinson, D., Adams, T., Duncan, A., Lee, S., *Characteristics of the Melt-Dilute Form of Aluminum-Based Spent Nuclear Fuel*, in *Savannah River Technology Center technical document, WSRC-TR-2002-00128*. 2002.
[2] McDeavitt, S., Abraham, D., Park, J., , *Evaluation of stainless steel-zirconium alloys as high-level nuclear waste forms.* Journal of Nuclear Materials, 1998. **257**: p. 21-34.
[3] Keiser, D., Abraham, D., Sinkler, W., Richardson, J., McDeavitt, S., *Actinide distribution in a stainless steel±15 wt% zirconium high-level nuclear waste form.* Journal of Nuclear Materials, 2000. **279**: p. 234-244.
[4] Janney, D.E., *Host phases for actinides in simulated metallic waste forms.* Journal of Nuclear Materials, 2003. **323**: p. 81–92.
[5] Olson, L., *Formulation of Reference Alloy Waste Form RAW-3, Savannah River National Laboratory Technical Document, SRNL-STI-2012-00534 and FCRD-SWF-2012-000348.* 2012.
[6] Ono, Y., Matsumoto, S., *Diffusion of Chromium, Manganese, and Nickel in Molten Iron.* Transactions of the Japan Institute of Metals, 1975. **16**: p. 415-422.
[7] Dayananda, M., Behnke, D., *Effective interdiffusion coefficients and penetration depths.* Scripta Metallurgica et Materialia, 1991. **25**(9): p. 2187-2191.
[8] Abraham, D.P., Richardson, J.W., McDeavitt, S.M., *Laves intermetallics in stainless steel–zirconium alloys.* Materials Science and Engineering A, 1997. **239-240**: p. 658–664.
[9] Fu, J., Yang, Y., Guo, J., Tong, W., *Effect of cooling rate on solidification microstructures in AISI 304 stainless steel.* Materials Science and Technology, 2008. **24**(8): p. 941-944.
[10] Fu, J., Yang, Y., Guo, J., Ma, J., Tong, W., *Microstructure evolution in AISI 304 stainless steel during near rapid directional solidification.* Materials Science and Technology, 2009. **25**(8): p. 1013-1016.
[11] *Application of the Schaeffler diagram*, https://dacapo.com/assets/download/tech/schaeffler_diagram.pdf, 2018.
[12] Kassner, M., Peterson, D., ed. *Phase diagrams of binary actinide alloys*. Monograph series on alloy phase diagrams, ed. Massalski. 1995, ASM International: Materials Park, OH 44073. 489.